Okamoto et al. Earth, Planets and Space 2014, 66:33
http://www.earth-planets-space.com/content/66/1/33

Earth, Planets and Space
a SpringerOpen Journal

LETTER Open Access

Distribution of CO_2 fluids in the Shimanto belt on Muroto Peninsula, SW Japan: possible injection of magmatic CO_2 into the accretionary prism

Atsushi Okamoto[1*], Michimasa Musya[1], Yoshitaka Hashimoto[2] and Noriyoshi Tsuchiya[1]

Abstract

Carbon dioxide and methane are major components in geofluids; however, there is little evidence showing how C-H-O fluids evolve in a subduction zone. We investigated fluid inclusions in quartz veins from the Eocene-Oligocene Shimanto belt (Murotohanto subbelt) on Muroto Peninsula, SW Japan using microthermometry and laser Raman spectroscopy. Quartz veins that cut the cleavage of the host rocks in the Murotohanto subbelt contain one-phase carbonic inclusions (CH_4) and two-phase aqueous inclusions ($CH_4 \pm CO_2$ vapor and H_2O liquid). The vapor in the two-phase inclusions is essentially CH_4 in the northern part of the belt and a CO_2-CH_4 mixture in the southern part; values of X_{CO_2} (=CO_2 / ($CO_2 + CH_4$)) vary from 0 to 0.9. Within a single CO_2-bearing vein, X_{CO_2} values decrease from the vein wall (X_{CO_2} = 0.5 to 0.9) to the vein center (X_{CO_2} = 0), and the homogenization temperature increases from approximately 180°C to 240°C-250°C, indicating a transition of the carbonic species from CO_2-CH_4 to CH_4 during vein formation. CO_2-dominant fluids are rare in most accretionary prisms formed under low-grade metamorphic conditions, and the generation of CO_2 cannot be explained by diagenesis of organic matter in sediments under the *P-T* conditions of formation of the CO_2-bearing veins (235°C to 245°C, 165 to 200 MPa). The CO_2 fluids are distributed preferentially near an out-of-sequence thrust that brings the Murotohanto subbelt into contact with the late Oligocene-early Miocene Nabae subbelt and its many volcanic and intrusive rocks. We therefore suggest that the CO_2 fluids were generated in association with near-trench magmatism during the middle Miocene and that the fluids were injected and mixed with the CH_4 pore fluids of the sediments in the accretionary prism.

Keywords: C-H-O fluid; Fluid inclusion; Shimanto belt; Magmatic CO_2; Quartz vein

Findings

Introduction

Fluids in the crust consist mainly of water, carbon dioxide, and methane, as well as electrolytes, and they may be carried down into the Earth's interior at subduction zones. The dominant volatiles in the pore fluids of sediments evolve during plate subduction, and based on thermodynamic calculations of C-H-O fluids coexisting with graphite at geologically common oxidation conditions, the dominant species changes from methane to water to carbon dioxide with increasing temperature (e.g., Holloway 1984). In accretionary prisms, the volatile species are products of microbial activity, hydrothermal water-rock interactions, or thermal decomposition of organic matter under low-grade metamorphic conditions (e.g., Tissot and Welte 1984).

The evolution of fluids during low-grade metamorphism has been studied extensively by analyzing fluid inclusions in the fissure quartz of the Central Alps, Switzerland (e.g., Mullis et al. 1994; Tarantola et al. 2007, 2009), and four fluid zones that correlate with increasing metamorphic conditions have been identified. These zones are a hydrocarbon zone formed at temperatures lower than 200°C, a methane zone formed at temperatures ranging from 200°C to 270°C, a water zone formed at temperatures in excess of 270°C, and a carbon dioxide zone at even higher temperatures. However, there is no direct evidence for a transition from CH_4 to CO_2 during prograde metamorphism.

* Correspondence: okamoto@mail.kankyo.tohoku.ac.jp
[1]Graduate School of Environmental Studies, Tohoku University, Sendai 980-8579, Japan
Full list of author information is available at the end of the article

Many studies have examined fluid inclusions in various ancient accretionary prisms formed under low-grade metamorphic conditions (e.g., Fisher and Brantley 1992; Moore and Vrolijk 1992; Sakaguchi 1996; Hashimoto et al. 2002, 2012; Kondo et al. 2005; Raimbourg et al. 2014), and they showed that methane is the only carbonic species in the fluids. Given this general lack of variety in the carbonic species found, it is not surprising that there is still little information on the variation in the chemistry of C-H-O fluids along subduction zones.

The Shimanto belt is one of the best-studied ancient accretionary complexes in the world (Taira et al. 1988). The metamorphic temperatures of the Shimanto belt ranged from 100°C to 300°C (e.g., Underwood et al. 1993; Sakaguchi 1996; Hashimoto et al. 2002, 2012; Kondo et al. 2005; Raimbourg et al. 2014), which overlaps the temperature range proposed for the seismogenic zone along subduction zones (100°C to 350°C; Hyndman and Wang 1993). Except at one locality on Muroto Peninsula, SW Japan, the carbonic component of the fluids in the Shimanto belt is always CH_4 (e.g., Hashimoto et al. 2002, 2012; Kondo et al. 2005; Raimbourg et al. 2014). At the locality on Muroto Peninsula, quartz veins contain a mixture of CO_2 and CH_4 vapor in two-phase aqueous inclusions (Lewis et al. 2000; Lewis and Byrne 2003). However, the origin and distribution of CO_2 fluids in the Shimanto belt remain unclear.

In the present study, we investigated the C-H-O compositions and homogenization temperatures of fluid inclusions in the mineral veins of the Eocene-Oligocene Shimanto belt on Muroto Peninsula. We revealed the spatial distribution of CO_2 fluids on both the regional and single-vein scale, and we discuss the possibility of CO_2 injection related to middle Miocene magmatism.

Geological background and occurrences of veins

The Shimanto belt crops out on the Pacific side of Japan from the Kanto region to the Ryukyu arc, a distance of approximately 1,000 km (Figure 1a). The belt is generally subdivided by the Aki tectonic line into two parts: the Cretaceous Shimanto belt in the north and the Paleogene-Neogene Shimanto belt in the south (Figure 1a,b). The Paleogene-Neogene Shimanto belt is composed mainly of packages of coherent trench-fill sediments (sandstone/shale) and lesser amounts of tectonic mélange (e.g., Taira et al. 1988). The Eocene to Oligocene Murotohanto subbelt (Figure 1b) is composed of E-W- to NE-SW-striking strata, and its contact with the late Oligocene to early Miocene Nabae subbelt to the south is marked by an out-of-sequence thrust (the Shiina-Narashi fault; Figure 1b).

Ditullio and Byrne (1990) described the polyphase deformation of the Paleogene-Neogene Shimanto belt in the following order: (1) synsedimentary deformation, (2) penetrative cleavage formation due to solution mass transfer, and (3) syn- to post-cleavage shearing and deformation. Vitrinite reflectance and illite crystallinity show that the peak temperature of the Murotohanto subbelt increased from north (approximately 215°C to 230°C) to south (270°C to 290°C) (DiTullio et al. 1993; Underwood et al. 1993). Across the Shiina-Narashi fault to the south, the peak temperature dropped from 270°C-290°C to 135°C-205°C. The Nabae subbelt is made up of several mélanges with pillow lavas, volcanic breccias, and intrusive gabbros and dolerites. Based on structural, chronological, and geochemical studies (e.g., Hibbard and Karig 1990; Mizoguchi et al. 2009), these igneous rocks are interpreted to have formed in association with near-trench magmatism during the middle Miocene (approximately 15 Ma). Offshore, the active equivalent of the Shimanto belt is referred to as the Nankai wedge (Figure 1a).

We collected mineral veins hosted by sedimentary rocks from eight localities in the Murotohanto subbelt, along the eastern (E1 to E3) and western (W1 to W5) coasts of Muroto Peninsula (Figure 1b). Localities W1, W5, and E1 are the same as those investigated by Lewis et al. (2000) and Lewis and Byrne (2003); CO_2-CH_4 fluids were reported only at locality W5. In the north (W1, W2, E1, and E2), thick sandstone layers are widespread, and mineral veins are rare and thin (<5 mm thick). In the south, sandstones and shales are intercalated with each other. Some of the rocks at locality W5 have a block-in-matrix structure. There are two types of veins: veins cutting sandstone blocks at high angles to bedding that do not continue into adjacent mudstone layers and veins cutting the cleavages of both mudstone and sandstone, indicating formation after the cleavage (i.e., post-cleavage veins). In this study, we focused on the post-cleavage veins hosted mostly by sandstones (Figure 2a). Most of the analyzed post-cleavage veins are extensional cracks, with a minor amount of shear displacement. The width of the veins commonly ranges from 0.01 to 100 mm, and the length is less than approximately 2 m.

We also analyzed a quartz vein hosted by pillow lava at locality E4 (Figures 1b and 2b). This sample was taken from a large floating block, interpreted to have been derived from Shiina volcanic rocks (e.g., Hibbard and Karig 1990; Mizoguchi et al. 2009). The Shiina volcanic rocks have been interpreted as intrusions into the Hioki mélange in the Miocene Nabae subbelt (Mizoguchi et al. 2009).

Fluid inclusions

Occurrences and compositions of fluid inclusions

We prepared doubly polished thin sections of the veins, cut perpendicular to the vein walls. The compositions of the fluid inclusions were measured by laser Raman microprobe spectroscopy (Kaiser Optical system, HoloLab 5000,

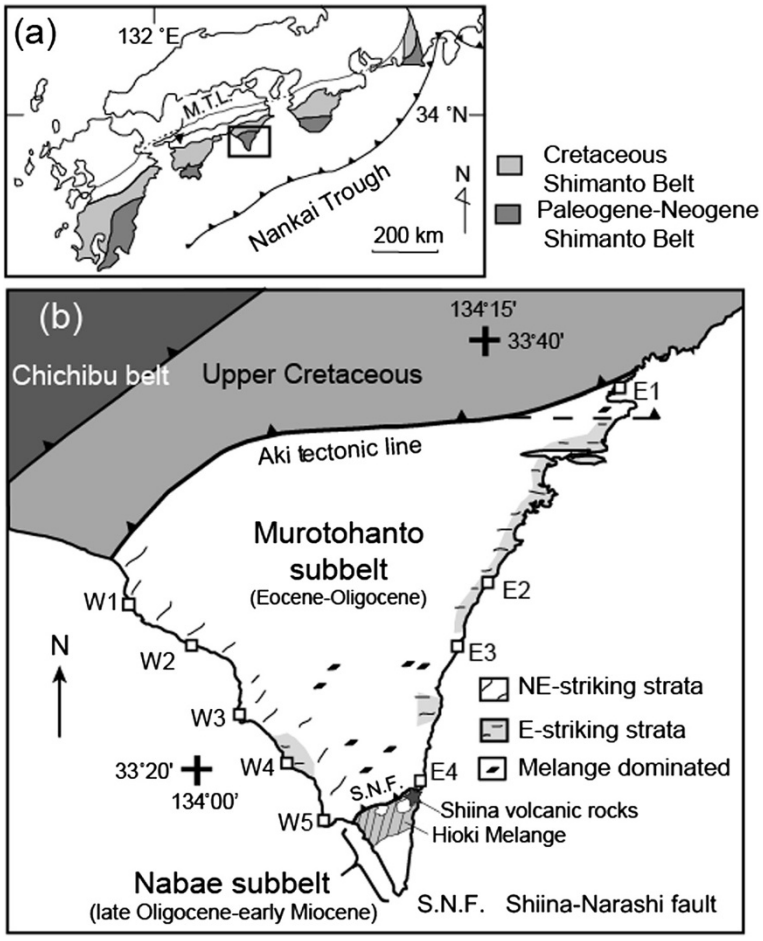

Figure 1 Distribution of the Shimanto belt and geological map of the Murotohanto subbelt. (a) Distribution of the Shimanto belt in SW Japan. **(b)** Geological map of the Murotohanto subbelt (Eocene-Oligocene) on Muroto Peninsula (after Lewis et al. 2000) showing sample localities along the eastern (E1 to E4) and western coasts (W1 to W5). Sample E4 was taken from a large *ex situ* block of pillow lava interpreted to be from the Miocene Shiina volcanic rocks within the Nabae subbelt (e.g., Hibbard and Karig 1990; Mizoguchi et al. 2009).

Ann Arbor, MI, USA). The size of the laser spot on the sample surface was about 2.0 μm. The veins are composed of quartz, and some also contain minor calcite. They include many primary, pseudo-secondary, and secondary inclusions, and most of these inclusions are smaller than 10 μm. For this study, we focused on the primary and pseudo-secondary inclusions. Representative Raman spectra of the fluid inclusions are shown in Additional file 1: Figure S1.

Except for sample E4 (hosted by pillow lava), the quartz veins contain two types of inclusions: one-phase carbonic inclusions and two-phase aqueous inclusions (Figure 2c). The one-phase carbonic inclusions have a smoky appearance (Figure 2c) and show a Raman band for CH_4 at 2,918 cm^{-1}. The two-phase aqueous inclusions are composed of liquid and vapor (Figure 2c), and they show a broad band around 3,200 to 3,600 cm^{-1}, indicating liquid H_2O. Vapors in the two-phase inclusions show either a sharp band for CH_4 or bands for both CH_4 (at 2,918 cm^{-1}) and CO_2 (at 1,287 and 1,389 cm^{-1}). The secondary inclusions contain only CH_4 vapor; CO_2 is not present.

Quartz veins in sample E4 (Shiina volcanics) also contain two-phase aqueous inclusions, but they do not contain one-phase inclusions. The vapor in the two-phase inclusions is entirely CO_2.

Variations of X_{CO_2} and T_h within the Murotohanto subbelt

The molar proportions of CH_4 and CO_2, X_{CO_2} = CO_2 / (CO_2 + CH_4), in the vapor of the two-phase inclusions were determined from the intensity (peak area) ratios of the CO_2 and CH_4 Raman spectra following the method of Burruss (2003). The error of the X_{CO_2} estimates is within approximately 0.1. The intensity data of the CO_2 and CH_4 bands and calculated X_{CO_2} are listed in Additional file 1: Table S1.

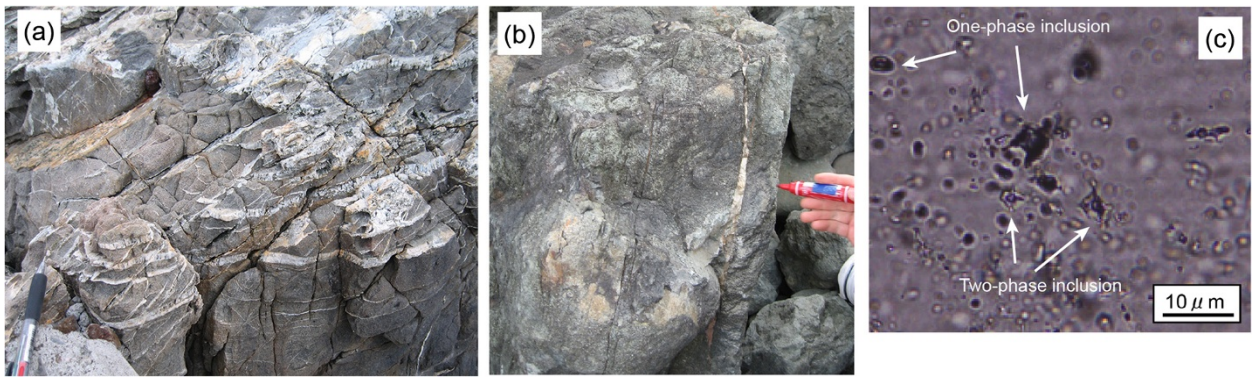

Figure 2 Outcrop photographs and optical photomicrograph. Outcrop photographs of quartz veins in **(a)** the sandstones at locality W1 and **(b)** the pillow lava block at locality E4. **(c)** Optical photomicrograph of one-phase carbonic and two-phase aqueous fluid inclusions in quartz crystals in veins.

The X_{CO_2} values in the Murotohanto subbelt change from north to south (Figure 3), and similar systematic changes occur along the western and eastern coasts of Muroto Peninsula. This indicates that the fluid distribution was affected by the structure of the accretionary complex (E-W- to NE-SW-trending strata; Figure 1). In the north (W2, E1, and E2), the vapor in the two-phase aqueous inclusions is CH_4 (X_{CO_2} = 0), although a vein at locality W1 contains a small amount of CO_2 (X_{CO_2} < 0.3; Figure 3). In contrast, the veins in the south (W3, W4, W5, and E3) contain a CH_4-CO_2 vapor with a wide range of X_{CO_2} values from 0 to 0.9 (Figure 3). We also note that all post-cleavage veins, hosted by the sedimentary rocks, contain pure CH_4 inclusions, even in the sample that possesses inclusions with high values of X_{CO_2}. In contrast, the quartz vein in the Shiina volcanic rocks (E4) contains only pure CO_2 vapor in its inclusions (Figure 3).

The homogenization temperatures (T_h) of the two-phase aqueous inclusions were measured by heating experiments with five samples (W1, W4, W5, E1, and E3; Figure 4a,b,c,d,e), and the temperatures scatter over the range of 180°C to 270°C. The mean values of homogenization temperature for the northern samples are 216°C ± 16°C (1σ) for W1 and 212°C ± 11°C for E1 (Figure 4a,d), and the mean values for the southern samples are 10°C to 20°C higher than those in the north (T_h = 223°C ± 22°C for W4, 236°C ± 14°C for W5, 226°C ± 15°C for E3) (Figure 4b,c,e). In Figure 4, sample E1 contains pure CH_4 vapor, whereas the other samples (W1, W4, W5, and E3) contain vapors of pure CH_4 and CH_4-CO_2 mixtures (Figure 3). The gray columns in Figure 4b indicate the T_h of the CH_4-only region (241°C ± 5°C) of sample W4.

The homogenization temperatures (T_c) of the one-phase carbonic inclusions (CH_4) were measured by cooling experiments with samples E1 and W4 (Figure 4f). Methane

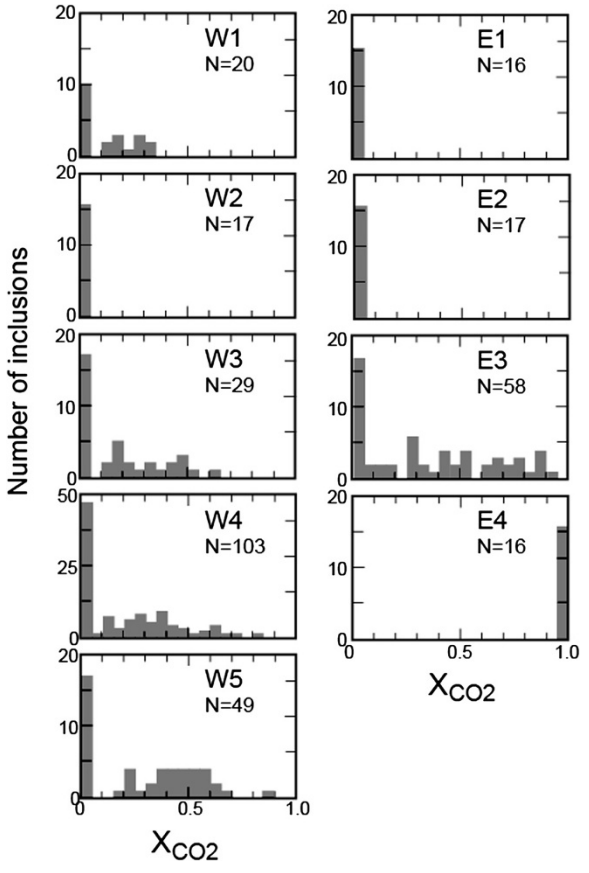

Figure 3 Histogram showing the molar proportions of CH_4 and CO_2, X_{CO_2} (=CO_2 / (CO_2 + CH_4)). In fluid inclusions from the eight localities on Muroto Peninsula. The X_{CO_2} value was determined from Raman spectra following the method of Burruss (2003).

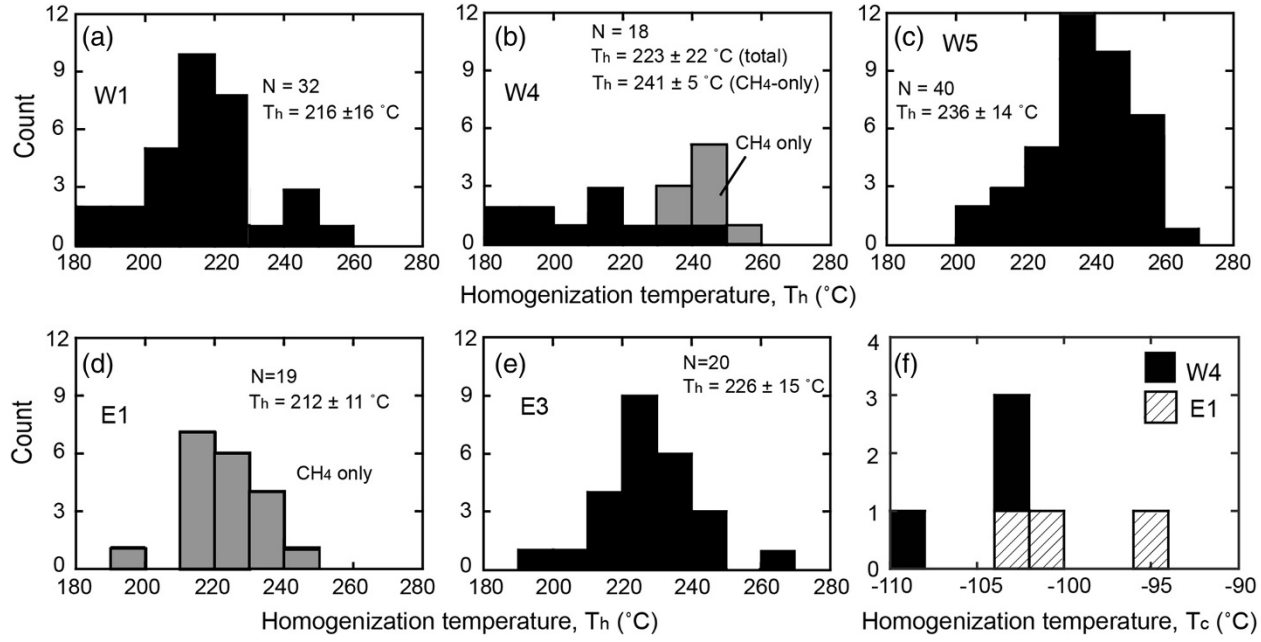

Figure 4 Homogenization temperatures. Homogenization temperatures (T_h) of the two-phase aqueous inclusions in veins from localities **(a)** W1, **(b)** W4, **(c)** W5, **(d)** E1, and **(e)** E3. In each histogram, the mean value with a standard deviation of 1σ is shown. **(f)** Homogenization temperatures (T_c) of the one-phase carbonic inclusions (CH_4) for samples W4 and E1. The veins in sample W4 contained both CH_4-only inclusions and CH_4-CO_2 mixtures. We identified the CH_4-only region in the vein and measured T_h (d) and T_c (f).

bubbles were observed below −90°C, and solid carbon dioxide was not observed. T_c was determined as the temperature at which the methane bubbles disappeared during re-heating of the inclusions.

Variations of X_{CO_2} and T_h within a single vein

We carried out detailed analyses of fluid inclusions in a single vein from locality W4. The post-cleavage vein is hosted by sandstone, and it is 8.2 mm wide and >1 m long. It is composed mainly of elongate crystals of quartz that have their long axes oriented subperpendicular to the vein walls (Figure 5a); the crystals grew from both walls and impinged near the center of the vein. A scanning electron microscopy cathodoluminescence (SEM-CL) image of the vein revealed euhedral crystal growth of the quartz near the vein wall (white arrows in Figure 5b); there are numerous microcracks in the center of the vein. Near the vein walls, a small amount of calcite fills the spaces between euhedral quartz crystals (Figure 5b). The quartz vein texture suggests that euhedral quartz crystals grew from the vein wall into open cavities during the initial stage of vein formation and that a repeated crack-seal process occurred to produce the elongate crystals.

Across the vein, the values of X_{CO_2} in the two-phase aqueous inclusions (line A to B in Figure 5a) show symmetrical patterns with respect to the central plane of the vein (Figure 5c). Near the vein wall (less than approximately 1.0 mm from the vein wall), where growth zoning of quartz is clear (Figure 5b), the vapor in the fluid inclusions is dominated by CO_2 with X_{CO_2} values ranging from 0.5 to 0.9 (Figure 5c). The X_{CO_2} value decreases toward the center of the vein, and the vapor is entirely CH_4 in the central part of the vein (3 to 6 mm from the vein walls) (Figure 5c). The one-phase carbonic inclusions, which are made up of CH_4 regardless of position within the vein, are distributed uniformly across the vein (Figure 5c).

The homogenization temperature of the two-phase inclusions, T_h, changes across the vein: the T_h value is 180°C to 200°C near the vein walls but increases to 240°C to 250°C at the vein center (Figure 5c). In summary, X_{CO_2} decreased and homogenization temperature, T_h, increased during the growth of the vein.

P-T conditions of vein formation

The pressure and temperature conditions of formation of the post-cleavage veins were estimated on the basis of fluid inclusion analyses (Figures 3, 4 and 5). When one-phase carbonic inclusions of CH_4 coexist with the two-phase aqueous inclusions with pure CH_4 vapor (X_{CO_2} = 0), the homogenization temperature (T_h) of the two-phase aqueous inclusions directly indicates the fluid trapping temperature (Vrolijk et al. 1988), because the value of T_h is consistent with the temperature of methane

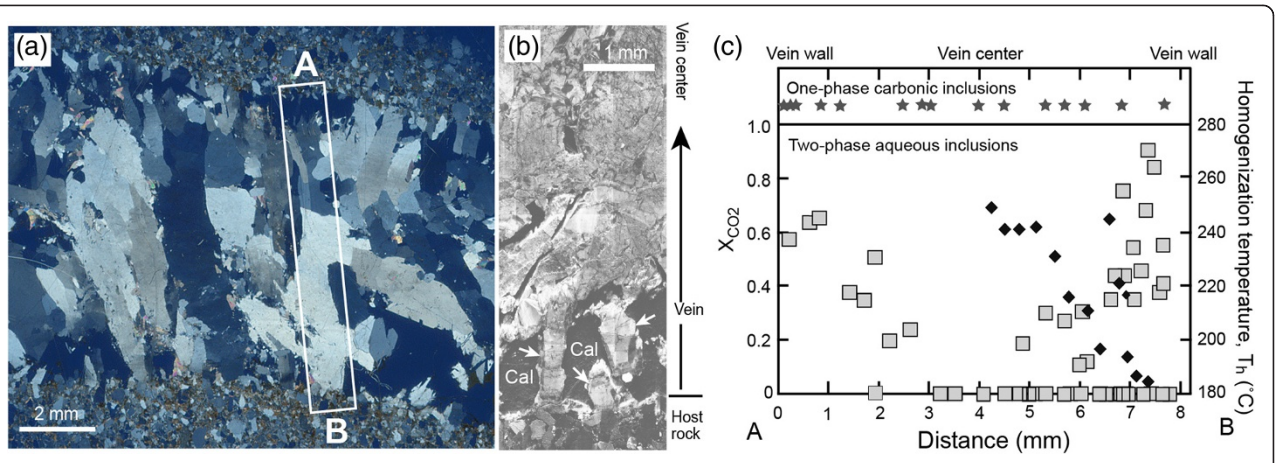

Figure 5 Variation of fluid compositions and homogenization temperatures (T_h) in a vein from locality W4. (a) Photomicrograph of the quartz vein in which elongate crystals grew inward from both walls and impinged at the center of the vein. **(b)** SEM-CL image of the same vein in the region from the vein wall to the vein center. Cal, calcite. **(c)** Variations of X_{CO_2} (=CO_2 / (CO_2 + CH_4)) (gray squares) and homogenization temperature (black diamonds) in two-phase aqueous inclusions across the vein (A to B in (a)). Note that the homogenization temperatures were measured in only one half of the vein along A to B. Gray stars indicate the positions of one-phase carbonic inclusions (CH_4) in the vein.

saturation in water. Given the trapping temperatures of the two-phase aqueous inclusions, pressures were determined by calculating isochores for the one-phase carbonic inclusions from cooling experiments (Vrolijk et al. 1988). In the cases where $X_{CO_2} > 0$, the T_h value indicates the minimum possible trapping temperature. Although great care is needed to identify cogenetic trapping of fluid inclusions (Raimbourg et al. 2014), we believe that the aqueous and carbonic fluid inclusions coexisted with each other in the analyzed veins because (1) both inclusions always exist in all the analyzed veins (except for sample E4), (2) they have close spatial associations in single crystals (Figure 2c), and (3) the aqueous inclusions contain $CH_4 \pm CO_2$ vapor.

We estimated the *P-T* conditions for samples E1 in the north and W4 in the south. In both veins, two-phase aqueous inclusions coexist with one-phase carbonic inclusions (Figure 2c). The vapor in the two-phase inclusions of sample E1 is always CH_4 (X_{CO_2} = 0; Figure 3). In contrast, the vein in sample W4 has variable X_{CO_2} values (Figures 3 and 5), and we therefore only measured the homogenization temperatures (T_h and T_c) at the center of the vein, where the vapor in most two-phase aqueous inclusions was pure CH_4 (X_{CO_2} = 0) (Figure 5c). Figure 6a shows the *P-T* conditions for samples E1 and W4. The error bars indicate the standard deviations of T_h, and individual pressures were obtained from the isochores of individual T_c values of the one-phase carbonic inclusions. The *P-T* conditions for W4 (235°C to 245°C, 165 to 200 MPa) are slightly higher than those for E1 (200°C to 220°C, 125 to 160 MPa). The temperatures of post-cleavage vein formation at locality W1, determined by Lewis et al. (2000), are similar to the temperature estimates of this study, but their pressures are approximately 50 MPa lower (Figure 6a). The *P-T* conditions of vein formation determined in this study and by Lewis et al. (2000) are plot between lithostatic and hydrostatic conditions along a geothermal gradient of approximately 35°C/km (Figure 6a).

Discussion and conclusions

It is important to consider the origin of the CO_2 fluids within the Murotohanto subbelt because CH_4 is the dominant carbonic component of fluids under low-grade metamorphic conditions in other parts of the Shimanto belt (e.g., Sakaguchi 1996; Hashimoto et al. 2002, 2012; Kondo et al. 2005), in ancient accretionary prism complexes (e.g., Fisher and Brantley 1992; Moore and Vrolijk 1992), and in active accretionary prisms (e.g., Tsunogai et al. 1998; Mau et al. 2006).

Tarantola et al. (2007, 2009) showed that the thermal conversion of CH_4 into CO_2 and H_2O occurred at 270°C ± 5°C in Alpine fissure quartz. Lewis and Byrne (2003) suggested that the CO_2 fluids in the Murotohanto subbelt were produced by thermal conversion of CH_4, as in Alpine fissure quartz, based on the facts that temperature increases from north to south in the Murotohanto subbelt (Underwood et al. 1993) and that pure CH_4 occurs in the north, but CH_4-CO_2 mixtures occur in the south. However, we reject this scenario because (1) the fluid in the post-cleavage veins of the Murotohanto subbelt was initially dominated by CO_2 and then changed to CH_4 (Figure 5), (2) the temperature of the vein formation (200°C to 250°C; Figure 6a) is lower than the temperature of the thermal conversion proposed by Tarantola et al. (2007, 2009) (270°C ± 5°C), and (3) only CH_4 fluids were found in even the higher-grade parts of the Shimanto belt (>300°C

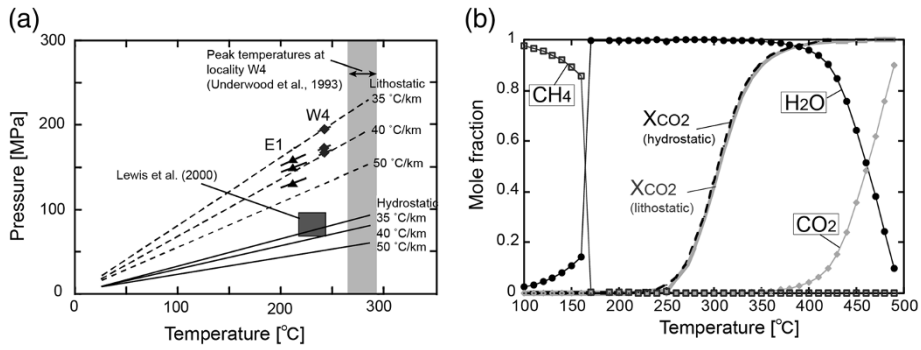

Figure 6 *P-T* conditions of vein formation and fractions of chemical species. (a) *P-T* conditions of vein formation estimated from microthermometry for the two-phase inclusions with only CH_4 vapor and the one-phase carbonic inclusions. The gray square indicates the *P-T* condition of fluid inclusions at locality W1 estimated by Lewis and Byrne (2003). The light-gray zone indicates the peak temperature around locality W4 based on vitrinite reflectance (Underwood et al. 1993). **(b)** The fractions of chemical species in the C-H-O fluids in equilibrium with graphite, buffered by the reaction among quartz, magnetite, and fayalite, along the geothermal gradient of 35°C/km (lithostatic) determined by using the Perple_X computer program package (Connolly 1995). X_{CO_2} indicates the molar ratio of CO_2 / (CO_2 + CH_4). The profile of X_{CO_2} with depth under the lithostatic condition (black broken curve) is similar to that under the hydrostatic condition (gray bold curve).

at the Nobeoka thrust; Kondo et al. 2005). Figure 6b shows the thermodynamic calculations obtained by using the Perple_X computer program package (Connolly 1995) for the mole fractions of C-H-O species coexisting with graphite under the quartz-fayalite-magnetite (QFM) buffer along the geothermal gradient of vein formation (35°C/km, lithostatic). This diagram shows that the dominant species changes with increasing temperature from CH_4 ($T < 170$°C) to H_2O (170°C < T < 450°C) to CO_2 ($T >$ 450°C) and that X_{CO_2} is very low (<0.1) at the temperatures of vein formation (200°C to 250°C; Figure 6a) under both lithostatic and hydrostatic conditions. Therefore, diagenesis of organic matter in the sediments is unlikely to explain the origin of the CO_2.

The veins and host rocks in the Shimanto belt commonly contain calcite (e.g., Okamoto and Sekine 2011). Decarbonation reactions in carbonate-bearing metasediments could occur at temperatures less than approximately 350°C (e.g., Massone, 2010). Therefore, it is possible that CO_2 fluids were generated by decarbonation reactions in the deeper part of the subduction zone and then transported to shallower levels. Although this scenario cannot be ruled out, it is difficult to explain by decarbonation reactions why CO_2-bearing fluids are distributed only in the south of the Murotohanto subbelt. In addition, the unmixing of CH_4-CO_2-H_2O fluids from deeper regions cannot explain the variation of X_{CO_2} in the analyzed vein (Figure 5) because separation of CH_4-rich fluid by unmixing would cause an increase of X_{CO_2} in the aqueous fluids, which contradicts the X_{CO_2} decrease during the growth of the analyzed vein (Figure 5c).

An alternative source of CO_2 fluids is magmatism in the vicinity of the accretionary prism. Discharge of CO_2 from hydrothermal vents associated with submarine volcanoes has been reported in various places, including the Okinawa trough (Konno et al. 2006), the Izu-Bonin-Mariana and Tonga-Kermadec arcs (Lupton et al. 2008), and the Mid-Atlantic Ridge in Iceland (Botz et al. 1999). Discharges of CO_2 can take the form of either liquid droplets or gas bubbles, depending on the pressure-temperature conditions of the site on the seafloor, and the vent fluids commonly have X_{CO_2} values exceeding 0.99. It is well known that basic and acidic igneous bodies are distributed widely within the Shimanto belt, and these igneous rocks have been dated as middle Miocene (approximately 15 Ma; e.g., Underwood et al. 1993). On Muroto Peninsula, such igneous rocks (pillow lava, volcanic breccia, dolerite, and gabbro) are not found in the Eocene-Oligocene Murotohanto subbelt but occur only within the late Oligocene to early Miocene Nabae subbelt. Based on plate reconstructions (Underwood et al. 1993), it is considered that such magmatic activities were related to the subduction of a young oceanic plate (Shikoku basin back-arc spreading ridge) in the middle Miocene.

The veins analyzed in this study cut the cleavage of the host rocks, which suggests that they formed later than the peak temperature conditions; however, the absolute timing of cleavage and vein formation within the Murotohanto subbelt remains unknown. Nevertheless, the rocks in the Murotohanto subbelt underwent a progressive deformation during and after the development of the out-of-sequence thrust (i.e., the Shinya-Narashi fault) that bounds the Murotohanto and Nabae subbelts (Ditullio et al. 1993; Underwood et al. 1993). In addition, pure CO_2 vapor is found in the inclusions only in the Shiina volcanic rocks, close to the Shinya-Narashi fault (Figure 3).

These facts support the hypothesis of CO_2 injection during the middle Miocene according to the following scenario. In the Murotohanto subbelt, few veins formed

during the Eocene and Oligocene, because coherent units are widely distributed. In this area, the formation of post-cleavage veins was probably triggered by the near-trench magmatism during the middle Miocene. At that time, magmatic CO_2 fluids diffused along the out-of-sequence thrust and propagating fractures and mixed with CH_4 pore fluids to form CO_2-CH_4 fluids with high values of X_{CO_2} (Figures 3 and 5). The presence of CO_2 fluids at one locality in the north (W1) suggests an inhomogeneous nature of the fluid flow within the Murotohanto subbelt (Figure 3). Because the input of external CO_2 was a short-term event, the dominant carbonic component in the fluid changed progressively from CO_2 to CH_4, as was recorded within the single vein (Figure 5).

It remains to be determined whether the thermal structure of the Murotohanto subbelt is that of an Eocene-Oligocene accretionary prism or whether it is the result of overprinting in the middle Miocene (Underwood et al. 1993). In our study, we were able to show that the CO_2 fluids are distributed in the region up to 10 to 15 km from the Shinya-Narashi fault (W3, W4, W5, and E3; Figure 3). However, the trapping temperature of the fluid inclusions in the southern vein (235°C to 245°C for locality W4; Figure 6a) is lower than the maximum vitrinite reflectance temperature at the same locality (270°C to 290°C, Figure 6a; Underwood et al. 1993), implying negligible temperature overprinting due to fluid flows related to Miocene magmatism. Nevertheless, such an injection of magmatic fluids into an accretionary prism could occur during the subduction of a young plate, which may produce unique geochemical environments along the subduction zone.

Additional file

Additional file 1: Supplementary material. Figure S1. Representative Raman spectra of (a) the one-phase carbonic fluid inclusions, showing only the band of CH_4; (b) the two-phase aqueous inclusions with CH_4 vapor; (c) the two-phase aqueous inclusion with a mixture of CH_4 and CO_2 vapor; and (d) the two-phase aqueous inclusions with pure CO_2 vapor in sample E4 (Shiina volcanic rocks). **Table S1.** intensity data of Raman bands for CO2 and CH4 and X_{CO2} (=CO_2/(CO_2 + CH_4) values in the vapor of the two-phase fluid inclusions formt he Murotohanto subbelt. **Table S2.** homogenization temperatures of two-phase aqueous inclusions (T_h) and one-phase carbonic inclusions (T_c).

Competing interests
The authors declare that they have no competing interests.

Authors' contributions
AO drafted the manuscript. MM carried out the fluid inclusion studies. YH and NT participated in making discussion on the tectonic implications of fluid inclusions. All authors read and approved the final manuscript.

Acknowledgements
We thank A. Yamaguchi for providing information in the field about Muroto Peninsula and basaltic rocks. We also thank N. Hirano and N. Watanabe for the discussions. This study was supported by a Grant-in-Aid for Scientific Research on Innovative Areas (nos. 22109501, 24109701) from the Ministry of Education, Culture, Sports, Science, and Technology of Japan and by a Grant-in-Aid for Challenging Exploratory Research from the Japan Society for the Promotion of Science (no. 23654180) awarded to A. Okamoto.

Author details
[1]Graduate School of Environmental Studies, Tohoku University, Sendai 980-8579, Japan. [2]Department of Applied Science, Faculty of Scienc, Kochi University, Kochi 780-8520, Japan.

Received: 18 November 2013 Accepted: 14 April 2014
Published: 15 May 2014

References
Botz R, Winckler G, Bayer R, Schmitt M, Garbe–Schönberg D (1999) Origin of trace gases in submarine hydrothermal vents of the Kolbeinsey Ridge, north Iceland. Earth Planet Sci Lett 171:83–93

Burruss RC (2003) Raman spectroscopy of fluid inclusions. In: Samson I, Anderson A, Marshall D (eds) Fluid inclusions: analysis and interpretation. Short Course Series, vol 32. Mineralogical Association of Canada, Ottawa, pp 279–289

Connolly JAD (1995) Phase diagram methods for graphitic rocks and application to the system C-O-H-FeO-TiO_2-SiO_2. Contrib Mineral Petrol 119:94–116

DiTullio L, Byrne T (1990) Deformation paths in the shallow levels of an accretionary prism: the Eocene Shimanto belt of southwest Japan. Geol Soc Am Bull 102:1420–1438

DiTullio I, Laughland MM, Byrne T (1993) Thermal maturity and constraints on deformation from illite crystallinity and vitrinite reflectance in the shallow levels of an accretionary prism: Eocene–Oligocene Shimanto belt, southwest Japan. In: Underwood MB (ed) Thermal evolution of the Tertiary Shimanto Belt, Southwest Japan: an example of ridge–trench interaction, vol 273, Spec. Pap. Geol. Soc. Am., pp 63–82

Fisher DM, Brantley SL (1992) Models of quartz overgrowth and vein formation: deformation and episodic fluid flow in an ancient subduction zone. J Geophys Res 97:20043–20061

Hashimoto Y, Enjoji M, Sakaguchi A, Kimura G (2002) P–T conditions of cataclastic deformation associated with underplating: an example from the Cretaceous Shimanto complex, Kii Peninsula, SW Japan. Earth, Planets Space 54:1133–1138

Hashimoto Y, Eida M, Kirikawa T, Iida R, Takagi M, Furuya N, Nikaizo A, Kikuchi T, Yoshimitsu T (2012) Large amount of fluid migration around shallow seismogenic depth preserved in tectonic mélange: Yokonami mélange, the Cretaceous Shimanto Belt, Kochi, Southwest Japan. Island Arc 21:53–64

Hibbard JP, Karig DE (1990) Structural and magmatic responses to spreading ridge subduction: an example from Southwest Japan. Tectonics 9:207–230

Holloway JR (1984) Graphite-CH_4-H_2O-CO_2 equilibria at low grade metamorphic conditions. Geology 12:455–458

Hyndman RD, Wang K (1993) Thermal constraints on the zone of major thrust earthquake failure: the Cascadia subduction zone. J Geophys Res 98:2039–2060

Kondo H, Kimura G, Masago H, Ohomori-Ikehara K, Kitamura Y, Ikesawa E, Sakaguchi A, Yamaguchi A (2005) Deformation and fluid flow of a major out-of-sequence thrust located at seismogenic depth in an accretionary complex: Nobeoka thrust in the Shimanto Belt, Kyushu, Japan. Tectonics 24, TC6008

Konno U, Tsunogai U, Nakagawa F, Nakaseama M, Ishibashi J, Nunoura T, Nakamura K (2006) Liquid CO_2 venting on the seafloor: Yonaguni Knoll IV hydrothermal system, Okinawa Trough. Geophys Res Lett 33, L16607. doi:10.1029/2006GL026115

Lewis JC, Byrne TB (2003) History of metamorphic fluids along outcrop-scale faults in a Paleogene accretionary prism: implications for prism-scale hydrology. Geochem Geophys Geosyst 4: doi:10.1029/2002GC000359

Lewis JC, Byrne TB, Pasteris D, London D, Morgan GB (2000) Early tertiary fluid flow and pressure–temperature conditions in the Shimanto accretionary complex of south-west Japan: constraints from fluid inclusions. J Metamorph Geol 18:319–333

Lupton J, Lilley M, Butterfield D, Evans L, Embley R, Massoth G, Christenson B, Namamura K, Schmidt M (2008) Venting of a separate CO_2-rich gas phase from submarine arc volcanoes: example from the Mariana and Tonga–Kermadec arcs. J Geophys Res 113:B08S12, doi:10.1029/2007JB005467

Massone H-J (2010) Phase relations and dehydration behaviour of calcareous sediments at very-low to low grade metamorphic conditions. Periodico di Mineralogia 79:21–43

Mau S, Sahling H, Rehder G, Suess E, Linke P, Soeding E (2006) Estimates of methane output from mud extrusions at the erosive convergent margin off Costa Rica. Mar Geol 225:129–144

Mizoguchi S, Kiminami K, Imaoka T, Kamei A (2009) Miocene near-trench magmatism in the Cape Muroto area, Shikoku, SW Japan. J Geol Soc Jpn 115:17–30, in Japanese with English abstract

Moore JC, Vrolijk P (1992) Fluids in accretionary prisms. Rev Geophys 30:113–135

Mullis J, Dubessy J, Poty B, O'Neil J (1994) Fluid regimes during late stages of a continental collision: physical, chemical, and stable isotope measurements of fluid inclusions in fissure quartz from a geotraverse through the Central Alps, Switzerland. Geochim Cosmochim Acta 58:2239–2267

Okamoto A, Sekine K (2011) Texture of syntaxial quartz veins synthesized by hydrothermal experiments. J Struct Geol 33:1764–1775

Raimbourg H, Thiery R, Vacelet M, Ramboz C, Cluzel N, Le Traong E, Yamaguchi A, Kimura G (2014) A new method of reconstructing the P-T conditions of fluid circulation in an accretionary prism (Shimanto, Japan) from microthermometry of methane-bearing aqueous inclusions. Geochim Cosmochim Acta 125:96–109

Sakaguchi A (1996) High paleogeothermal gradient with ridge subduction beneath the Cretaceous Shimanto accretionary prism, southwest Japan. Geology 24:795–798

Taira A, Kato J, Tashiro M, Okumura M, Kodama K (1988) The Shimanto belt in Shikoku, Japan—evolution of Cretaceous to Miocene accretionary prism. Mod Geol 12:5–46

Tarantola A, Mullis J, Guillaume D, Vennemann T, Dubessy J, de Capitani C (2007) Oxidation of methane at the CH_4/H_2O–(CO_2) transition zone in the external part of the Central Alps, Switzerland: evidence from stable isotope investigations. Chem Geol 237:329–357

Tarantola A, Mullis J, Guillaume D, Dubessy J, de Capitani C, Abdelmoula M (2009) Oxidation of CH_4 to CO_2 and H_2O by chloritization of detrital biotite at 270 ± 5°C in the external part of the Central Alps, Switzerland. Lithos 112:497–510

Tissot BP, Welte DH (1984) Petroleum formation and occurrence. Springer-Verlag, Berlin, p 699

Tsunogai U, Ishibashi J, Wakita H, Gamo T (1998) Methane-rich plumes in the Suruga Trough (Japan) and their carbon isotopic characterization. Earth Planet Sci Lett 160:97–105

Underwood MB, Byrne T, Hibbard JP, DiTullio L, Laughland MM (1993) The effects of ridge subduction on the thermal structure of accretionary prisms: a tertiary example from the Shimanto belt of Japan. In: Underwood MB (ed) Thermal evolution of the Tertiary Shimanto Belt, Southwest Japan: an example of ridge–trench interaction, vol 273, Spec. Pap. Geol. Soc. Am., pp 151–168

Vrolijk P, Myers G, Moore JC (1988) Warm fluid migration along tectonic melanges in the Kodiak accretionary complex, Alaska. J Geophys Res 29:599–613

doi:10.1186/1880-5981-66-33
Cite this article as: Okamoto *et al.*: **Distribution of CO_2 fluids in the Shimanto belt on Muroto Peninsula, SW Japan: possible injection of magmatic CO_2 into the accretionary prism.** *Earth, Planets and Space* 2014 **66**:33.